Nuclear incompressibility and density dependent *NN* interactions in the folding model for nucleus-nucleus potentials

Dao T. Khoa,[1] G. R. Satchler,[2] and W. von Oertzen[3]
[1]*Department of Physics, Chung Yuan Christian University, Chung Li, Taiwan 32023, Republic of China*
[2]*Physics Division, Oak Ridge National Laboratory, Oak Ridge, Tennessee 37831-6373*
and Department of Physics & Astronomy, University of Tennessee, Knoxville, Tennessee 37996-1200
[3]*Bereich FK, Hahn-Meitner-Institut-GmbH, Glienicker Strasse 100, D-14109 Berlin, Germany*
(Received 11 December 1996)

A generalized version of density dependence has been introduced into the M3Y effective nucleon-nucleon (*NN*) interaction that was based on the *G*-matrix elements of the Paris *NN* potential. The density dependent parameters have been chosen to reproduce the saturation binding energy and density of normal nuclear matter within a Hartree-Fock scheme, but with various values for the corresponding nuclear incompressibility *K* ranging from 176 to 270 MeV. We use these new density dependent interactions in the folding model to calculate the real parts of α-nucleus and nucleus-nucleus optical potentials for those systems where strongly refractive scattering patterns have been observed. These provide some information on the potentials at short distances, where there is a strong overlap of the projectile and target density distributions, and hence where the density dependence of the interaction plays an important role. We try to infer, from careful optical model (OM) analyses, the sensitivity of the scattering data to different *K* values. Results obtained for elastic α scattering on targets ranging from ^{12}C to ^{208}Pb allow us to determine unambiguously that the *K* value favored in this approach is within the range of 240 to 270 MeV. Similar OM analyses have also been done on measurements of the elastic scattering of ^{12}C+^{12}C, ^{16}O+^{12}C, and ^{16}O+^{16}O at incident energies up to 94 MeV/nucleon. These data were found to be much less sensitive over such a narrow range of *K* values. This lack of sensitivity is due mainly to the smaller maximum overlap density which occurs for these systems, compared to that which is formed in an α-nucleus collision. This makes the effects of density dependence less substantial. Another reason is that a small difference between two folded heavy ion potentials can often be compensated for, in part, by a small overall renormalization of one of them. This renormalization is often allowed in optical model analyses, and interpreted, for example, as accounting for a contribution from a higher-order dynamic polarization potential. In an attempt to avoid this ambiguity, some OM analyses of the extensive and accurate data for ^{16}O+^{16}O scattering were done using the unrenormalized folded potentials, together with the explicit addition of a correction term, expressed in terms of cubic splines. This correction term can be interpreted as representing a contribution to the real potential from the dynamic polarization potential. The results of such a ''folding +spline'' analysis suggest a tendency to favor the same *K* value range that was found in the OM analyses of α-nucleus scattering. [S0556-2813(97)01008-X]

PACS number(s): 25.70.Bc, 21.30.Fe, 21.65.+f, 24.10.Hf

I. INTRODUCTION

Among various models for the heavy-ion (HI) interaction potential, the double-folding model [1,2] has been widely used to calculate the real parts of α-nucleus and nucleus-nucleus optical potentials. The folding model potential is identified as a representation of the first-order term of the formal optical potential given by Feshbach's reaction theory [3]. This potential is defined, when used in the one-body Schrödinger equation, to generate the relative motion part of that component of the total wave function of the HI system in which the two colliding nuclei remain in their ground states. That is, it describes their elastic scattering. Antisymmetrization of the system is taken into account to the extent that single-nucleon ''knock-on'' exchange terms are usually evaluated. The success of this approach in describing the observed elastic scattering of many systems suggests that it produces the dominant part of the real optical potential and that the real contributions from the couplings to the nonelastic channels, the ''dynamic polarization potential'' (DPP), are quite small except under special circumstances. Two such circumstances are when one nucleus is loosely bound and its breakup becomes important [4], or at low energies near the top of the Coulomb barrier when the DPP may become important: the so-called ''threshold anomaly'' [5].

The basic inputs to a folding calculation are the nuclear densities of the colliding nuclei and the effective nucleon-nucleon (*NN*) interaction. Once we have realistic nuclear densities, available from different nuclear models or directly from the electron-scattering data, it still remains necessary to have a realistic effective *NN* interaction before the success of the folding model can be reliably assessed. Popular choices for this have frequently been based upon the M3Y interactions which were designed to reproduce the *G*-matrix elements of the Reid [6] and Paris [7] *NN* potentials in an oscillator basis. We refer to these as the M3Y-Reid and M3Y-Paris interaction, respectively. The Reid version was used with some success in folding model calculations of the HI optical potential at relatively low energies [1]. These cases primarily probed the potential in the surface, near the

strong absorption radius. However, in cases of refractive nuclear scattering, characterized by the observation of ''rainbow'' features and seen first for α particles [8,9] and later on for other light HI systems (see, e.g., Refs. [10–12]), the scattering is sensitive to the optical potential over a wider radial domain [13,14]. Here, the simple M3Y-type interaction failed to give a good description of the data. The corresponding folded potentials were too deep at small internuclear distances to reproduce the rainbow features in the scattering cross section at the larger angles. However, because they were designed to reproduce the G matrix in an oscillator representation, i.e., matrix elements for a finite nucleus, the original M3Y interactions only correspond to an average over both kinetic energy and the density of the surrounding medium. This fact has motivated the inclusion into the original M3Y interactions of an explicit density dependence, to account for the reduction in the strength of the interaction that occurs as the density of the surrounding medium increases. An early version of the density dependence of the M3Y-Reid interaction was based upon the G-matrix calculations of Jeukenne *et al.* [15]. It was dubbed the DDM3Y interaction and greatly improved the description of the rainbow phenomena observed for α-nucleus scattering [16,17] as well as data for light HI scattering [18].

In a further development of the M3Y-type of interaction, a nuclear matter (NM) study within the Hartree-Fock (HF) scheme [19] has shown that the original density *independent* M3Y interaction [6,7] failed to saturate cold NM, leading to collapse. The introduction of a density dependence allows saturation to occur. However, the DDM3Y density dependence resulted in the correct binding energy (about 16 MeV/nucleon) but at the wrong density ($\rho_0 \simeq 0.07$ fm^{-3}, compared to the empirical saturation density of about 0.17 fm^{-3}). Therefore, several new density dependences for the M3Y interaction were introduced [19–21], with parameter values chosen to reproduce the observed NM saturation properties. Furthermore, we believe the later M3Y-Paris interaction to be more realistic, and we concentrate our attention on that. For example, a recent HF study of asymmetric NM [22] showed the M3Y-Paris interaction to give a more accurate description of the isospin dependence than does the M3Y-Reid version.

Although the different versions of density dependence give, by design, the same saturation properties, they do result in different *curvatures* of the binding energy curve $B(\rho)$ near the saturation point, i.e., they are associated with different values of the nuclear incompressibility,

$$K = 9\rho^2 \frac{d^2 B(\rho)}{d\rho^2}. \tag{1.1}$$

For example, the original DDM3Y interaction was associated with an exponential dependence on density [16],

$$F(\rho) = C[1 + \alpha \exp(-\beta\rho)], \tag{1.2}$$

chosen largely for its simplicity in folding calculations [1]. When the parameter values were adjusted to give the correct saturation properties with the M3Y-Paris interaction [20], this revised interaction (now known as DDM3Y1) yielded $K = 176$ MeV. Due to its exponential form, other solutions are not possible, so a more flexible power-law density dependence was introduced [19,20],

$$F(\rho) = C(1 - \alpha\rho^{\beta}). \tag{1.3}$$

A popular version of this form of density dependence uses $\beta = 2/3$ [24]. However, integer values of β allow for a simple separation of variables when these interactions are used to compute double-folded potentials and ρ is defined as $\rho = \rho_1 + \rho_2$. Hence attention was focused on these. Values of $\beta = 1$, 2, and 3 were explored, resulting in $K = 270$, 418, and 566 MeV, respectively. These new density dependent interactions were named BDM3Yβ, and have been used extensively in the folding model analysis of α-nucleus [20], as well as light HI [21,23], elastic scattering. A particular emphasis in these analyses has been put on the refractive scattering pattern observed at large angles, which is dominated by far-side scattering. For example, see in the upper part of Fig. 1 the optical model (OM) results [20] obtained for the $\alpha + {}^{40}$Ca system at 104 MeV using different versions of the interactions in comparison with data [25]. The decomposition of the elastic-scattering amplitude into the near- and far-side components (lower part of Fig. 1), using the technique suggested by Fuller [26], shows clearly a dominance of the far-side scattering at large angles. These (strongly refractive) data have been shown [27] to be sensitive to the $\alpha + {}^{40}$Ca potential at an internuclear distance as small as 2 fm. As a consequence, such data provide a severe test of different models for α-nucleus potentials [28].

The results of our folding analyses, especially those obtained for α-nucleus scattering [20], showed unambiguously that the most successful of the suggested density dependences were the DDM3Y1 and BDM3Y1 versions (see upper part of Fig. 1), which are associated with $K = 176$ and 270 MeV, respectively. The first choice corresponds to a nuclear equation of state (EOS) that is quite soft. At one time a very soft EOS was thought to be sufficient to allow a prompt explosion in supernovas [29], but more recent numerical studies indicate that this is not the case and current thought about supernovas explosions places less emphasis on the value of K [30]. The second choice of $K = 270$ MeV still corresponds to a relatively soft EOS. It had been hoped to gain some information on the EOS from the measured transverse flows of a variety of particles and nuclear fragments in high energy central HI collisions [31], but the results obtained so far [32] remain less conclusive than those obtained from our analyses of refractive scattering. A recent determination of K based upon the production of hard photons in HI collisions led to the estimate $K = 290 \pm 50$ MeV [33], which is close to the upper value that we obtained. Another approach to the determination of the incompressibility K for nuclear matter is to extrapolate from the energies of nuclear giant monopole resonances in finite nuclei. However, this procedure is also fraught with difficulty and a recent study [34] concluded that the present set of data only limits K to somewhere in the range from 200 to 350 MeV. Another study [35] argues that microscopic calulations of the monopole resonances remain the most reliable way of determining K for nuclear matter from the energies of monopole vibrations in finite nuclei. These authors conclude that the evidence indicates a compression modulus in the range 210 to

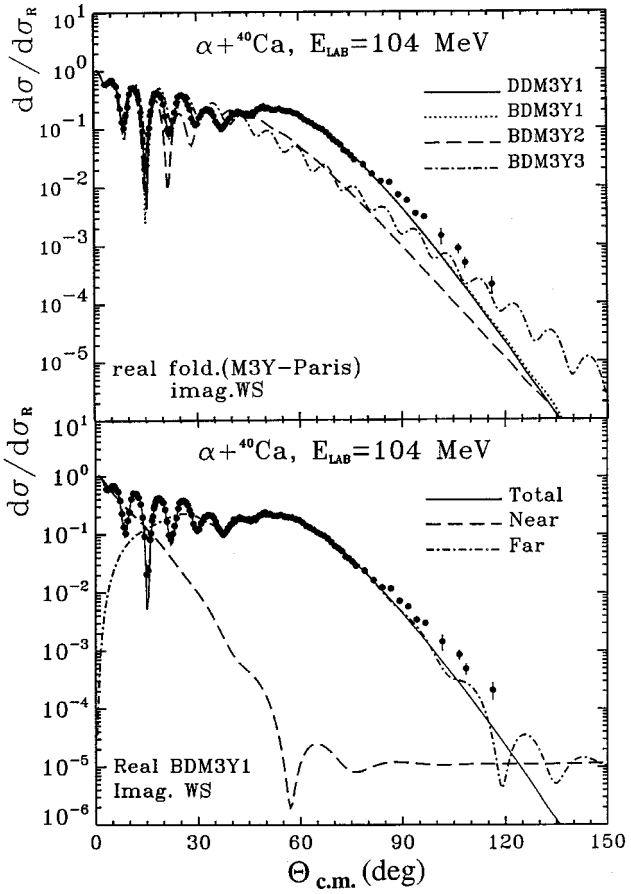

FIG. 1. Elastic $\alpha+{}^{40}$Ca scattering cross sections at $E_{\rm lab}=104$ MeV obtained with different real folded potentials (upper part), which were calculated using different density dependent interactions (see Ref. [20]). The best-fit DDM3Y1 and BDM3Y1 potentials were calculated using the interactions which yield the nuclear incompressibility $K=176$ and 270 MeV, respectively. Decomposition of the scattering amplitude (given by the BDM3Y1 potential) into the near- and far-side components (lower part) was done using the technique suggested in Ref. [26].

220 MeV. We also note that a fully microscopic description of nuclear matter within a relativistic Brueckner-Hartree-Fock theory [36], using the Bonn *NN* potential (type *A*), reproduces the NM saturation properties correctly and gives $K\simeq 290$ MeV.

The K values found by our previous folding model analyses, indicating that K falls within the range of about 170–270 MeV, are generally compatible with the values obtained from the other sources just discussed. Nonetheless, it remains desirable to see whether an empirical value can be determined more closely by our (folded) optical model approach. This has motivated us to study in more detail the density dependence of the effective NN interaction which is used as a key input in the folding model for nucleus-nucleus potentials. We do this by designing interactions associated with K values intermediate between those given by DDM3Y1 and BDM3Y1. At first sight, the simplest approach would be to introduce into the power-law form (1.3) values of β that are less than unity (for example, the density dependence (1.3) of the M3Y-Paris interaction, with a popular $\beta=2/3$, has been shown [22] to give $K=218$ MeV). However, as mentioned earlier, noninteger values of β do not lead to separation-of-variable properties that greatly simplify folding calculations; indeed the computation becomes considerably more complicated. Consequently, we chose a hybrid of the DDM3Y1 and BDM3Y1 forms, which allows us to explore intermediate values of K at the price of introducing one new parameter γ,

$$F(\rho)=C[1+\alpha\exp(-\beta\rho)-\gamma\rho]. \tag{1.4}$$

We chose parameter values which yielded K ranging from 188 to 252 MeV in roughly 10 MeV steps (see Table I). These intermediate sets were denoted CDM3Yn($n=1\rightarrow 6$) and their use allows us to trace in finer detail the sensitivity of refractive scattering data to the K value and thus, hopefully, determine it with more precision.

A brief description of the new parametrization of the density dependent interaction based on the HF results for the saturation properties of cold NM, as well as the main features of the double-folding model, are given in Sec. II. Results of our folding analyses of the elastic α-particle scattering data on different targets, using the real optical potential calculated with the new interactions, are discussed in Sec. III A. Those obtained for the elastic ^{12}C and ^{16}O scattering are discussed in Sec. III B. A summary and the main conclusions of the present work are given in Sec. IV.

II. THEORETICAL FORMALISM

A. Density dependent M3Y interaction in the HF calculation of nuclear matter

The effective in-medium nucleon-nucleon interactions frequently used in nuclear reaction calculations can be

TABLE I. Parameters [see Eq. (1.4)] of different density dependences $F(\rho)$ of the M3Y-Paris interaction. Values of the nuclear incompressibility K were obtained from the Hartree-Fock calculation of nuclear matter reported in Sec. II A.

Interaction	C	α	β (fm^3)	γ (fm^3)	K (MeV)
DDM3Y1	0.2963	3.7231	3.7384	0.0	176
CDM3Y1	0.3429	3.0232	3.5512	0.5	188
CDM3Y2	0.3346	3.0357	3.0685	1.0	204
CDM3Y3	0.2985	3.4528	2.6388	1.5	217
CDM3Y4	0.3052	3.2998	2.3180	2.0	228
CDM3Y5	0.2728	3.7367	1.8294	3.0	241
CDM3Y6	0.2658	3.8033	1.4099	4.0	252
BDM3Y1	1.2521	0.0	0.0	1.7452	270

roughly divided into two groups. In the first group one parametrizes the effective interaction directly (such as the Skyrme forces), leaving out any connection with a realistic free *NN* interaction. In the second group one first derives the effective interaction in the lowest-order of a many-body calculation (for example, a solution of the Bethe-Goldstone equation), starting from a realistic *NN* interaction which reproduces the free *NN* scattering data. This interaction is already dependent on the density of the NM, either explicitly (as in Ref. [15], for example), or in an average way because it was evaluated in a basis (such as oscillator wave functions) suitable for a finite nucleus (as was the case with the M3Y interactions). Then one can obtain a good description of the NM saturation properties in a simple HF calculation, by fine tuning the parameters for the density dependence. Like in our earlier studies [19–21], in the present work we have constructed an effective density dependent and local *NN* interaction by taking the original M3Y-Paris interaction, which represents an average over density, and introducing an explicit dependence $F(\rho)$ on density. The values of the parameters C, α, and β were then adjusted so as to reproduce, in HF approximation, the saturation properties of symmetric NM, namely, a binding energy per nucleon of $B(\rho_0)\simeq 16$ MeV at a saturation density $\rho_0\simeq 0.17$ fm^{-3}.

Let us first recall the main features of a HF calculation of the NM binding energy. With the direct (v_D) and exchange ($v_{\rm EX}$) parts of the interaction determined from the singlet- and triplet even ($v_{\rm SE}$, $v_{\rm TE}$) and odd ($v_{\rm SO}$, $v_{\rm TO}$) components of the M3Y two-nucleon forces [7], one obtains the ground-state energy of cold NM as

$$E=E_{\rm kin}+\frac{1}{2}\sum_{k\sigma\tau}\sum_{k'\sigma'\tau'}[\langle \mathbf{k}\sigma\tau,\mathbf{k}'\sigma'\tau'|v_D|\mathbf{k}\sigma\tau,\mathbf{k}'\sigma'\tau'\rangle + \langle \mathbf{k}\sigma\tau,\mathbf{k}'\sigma'\tau'|v_{\rm EX}|\mathbf{k}'\sigma\tau,\mathbf{k}\sigma'\tau'\rangle], \tag{2.1}$$

where $|\mathbf{k}\sigma\tau\rangle$ are ordinary plane waves. The direct v_D and exchange $v_{\rm EX}$ parts of the (central) *NN* forces can be written in terms of spin-isospin dependent components as

$$v_{D({\rm EX})}(r)=v_{00}^{D({\rm EX})}(r)+v_{10}^{D({\rm EX})}(r)\sigma\sigma'+v_{01}^{D({\rm EX})}(r)\tau\tau' + v_{11}^{D(EX)}(r)(\sigma\sigma')(\tau\tau'). \tag{2.2}$$

The explicit radial dependences of the M3Y-Paris interaction [7] can be given in terms of three Yukawas. In our case we need

$$v_{00}^{D}(r)=11061.625\frac{\exp(-4r)}{4r}-2537.5\frac{\exp(-2.5r)}{2.5r},$$

$$v_{00}^{\rm EX}(r)=-1524.25\frac{\exp(-4r)}{4r}-518.75\frac{\exp(-2.5r)}{2.5r} -7.8474\frac{\exp(-0.7072r)}{0.7072r}. \tag{2.3}$$

It has been shown [19] that the original (density *independent*) M3Y-type interaction fails to give saturation in NM. The introduction of a density dependent factor, $F(\rho)$, can avoid this difficulty [19,20],

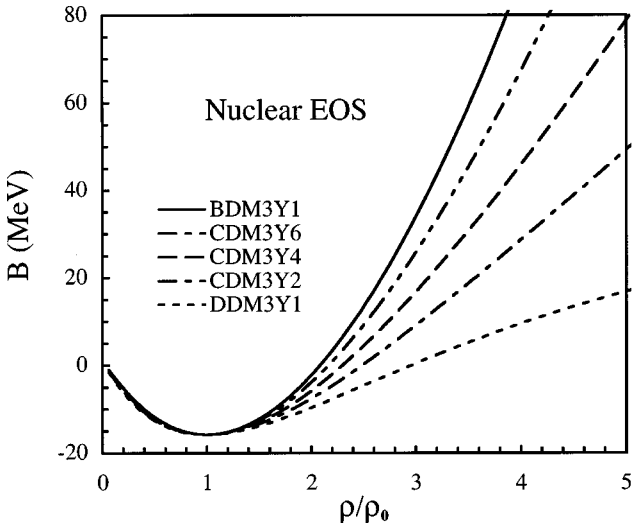

FIG. 2. Different EOS as generated by Hartree-Fock calculations of nuclear matter, using the new versions of the density dependent M3Y-Paris interaction proposed here which have been adjusted to give a saturation density of $\rho_0\simeq 0.17$ fm^{-3} and a saturation binding energy of 16 MeV per nucleon (see Table I).

$$v_{D({\rm EX})}(\rho,r)=F(\rho)v_{D({\rm EX})}(r). \tag{2.4}$$

As already discussed, the previous work [19,20] used either the form (1.2) or (1.3) for $F(\rho)$. Here we use the hybrid form (1.4), with a range of values for the mixture parameter γ. The corresponding values for C, α, and β to give the required saturation properties are collected in Table I, together with the predicted incompressibilities K. Now K varies smoothly from 176 MeV (DDM3Y1) to 270 MeV (BDM3Y1), a range which encompasses the value of around 210 MeV recently deduced [35]. The associated EOS are illustrated in Fig. 2. We have some hope of distinguishing between these if the scattering data are sensitive to the real optical potential at small internuclear separations that correspond to high overlap densities, approaching twice (or more) normal nuclear matter density.

B. Double-folding model for scattering

We give here only a short summary of the extended version of the folding model and refer to Ref. [23] for more details. In the present work, some minor modification has been introduced to the folding code used in Ref. [23] to handle the new (CDM3Y) form of the density dependence. In the first order of Feshbach's theory for the optical potential [3], the microscopic, antisymmetrized, nucleus-nucleus potential can be evaluated as a Hartree-Fock potential of the dinuclear system,

$$V=V_D+V_{\rm EX}=\sum_{i\in A_1,j\in A_2}[\langle ij|v_D|ij\rangle+\langle ij|v_{\rm EX}|ji\rangle], \tag{2.5}$$

where $|i\rangle$ and $|j\rangle$ refer to the single-particle wave functions of nucleons in the two colliding nuclei A_1 and A_2, respectively; v_D and $v_{\rm EX}$ are the direct and exchange parts of the effective *NN* interaction, as given in Eqs. (2.2) and (2.3).

The exchange potential $V_{\rm EX}$ accounts for the knockon interchange of the two interacting nucleons, one in the projectile and one in the target.

We emphasize that the potential V defined by Eq. (2.5) is the (real) first order term of the Feshbach optical potential. Experience has taught us that in many cases the contributions of higher order to the real potential are small [2], so that V, supplemented by an absorptive, imaginary term, and used in a one-body Schrödinger equation with the reduced mass of the two separated nuclei, is designed to generate a good approximation to the relative motion wave function of the two colliding nuclei while they remain in their ground states [3]. Due to the absorption into other, nonelastic channels, this may be only a small component of the total wave function, but it is that portion which describes the elastic scattering.

By introducing one-body density matrices $\rho_{1(2)}(\mathbf{r},\mathbf{r}')$ of the two colliding nuclei [with $\rho(\mathbf{r},\mathbf{r})\equiv\rho(\mathbf{r})$], one can explicitly write the direct and exchange potentials as

$$V_D(E,\mathbf{R})=\int \rho_1(\mathbf{r}_1)\rho_2(\mathbf{r}_2)v_D(\rho,E,s)d^3r_1d^3r_2,$$

$$\mathbf{s}=\mathbf{r}_2-\mathbf{r}_1+\mathbf{R}; \tag{2.6}$$

$$V_{\rm EX}(E,\mathbf{R})=\int \rho_1(\mathbf{r}_1,\mathbf{r}_1+\mathbf{s})\rho_2(\mathbf{r}_2,\mathbf{r}_2-\mathbf{s})$$

$$\times v_{\rm EX}(\rho,E,s)\exp\left[\frac{i\mathbf{k}(\mathbf{R})\mathbf{s}}{M}\right]d^3r_1d^3r_2. \tag{2.7}$$

Here $k(\mathbf{R})$ is the relative motion momentum given by

$$k^2(\mathbf{R})=\frac{2mM}{\hbar^2}[E_{\rm c.m.}-V(E,\mathbf{R})-V_C(\mathbf{R})], \tag{2.8}$$

where $M=A_1A_2/(A_1+A_2)$ is the reduced mass number, $E_{\rm c.m.}$ is the center-of-mass (c.m.) energy and m is the bare nucleon mass. $V(E,\mathbf{R})=V_D(E,\mathbf{R})+V_{\rm EX}(E,\mathbf{R})$ and $V_C(\mathbf{R})$ are the total nuclear and Coulomb potentials, respectively. The folded potential V is *nonlocal* through its exchange term and contains a self-consistency problem because k depends upon V. The exact treatment of the nonlocal exchange term is complicated numerically, but one may obtain an equivalent *local* potential by using a realistic approximation for the mixed density matrix [37]

$$\rho(\mathbf{R},\mathbf{R}+\mathbf{s})\simeq\rho\left(\mathbf{R}+\frac{\mathbf{s}}{2}\right)\hat{j}_1\left[k_F\left(\mathbf{R}+\frac{\mathbf{s}}{2}\right)s\right]$$

with

$$\hat{j}_1(x)=3(\sin x-x\cos x)/x^3. \tag{2.9}$$

The average local Fermi momentum k_F is chosen [37] so as to accelerate the convergence of the density-matrix expansion. Its explicit form is given in Ref. [23].

In the folding calculations (2.6) and (2.7), the density dependent interaction has also been assumed to be energy dependent, and we use the following form:

$$v_{D({\rm EX})}(\rho,E,r)=g(E)F(\rho)v_{D({\rm EX})}(r). \tag{2.10}$$

The energy dependent factor in Eq. (2.10) is taken to be a linear function of the bombarding energy E; $g(E)=1-0.003E/A$ for the M3Y-Paris interaction. It was introduced phenomenologically [19] to account for an explicit (rather weak) energy dependence of the effective interaction required to reproduce the empirical energy dependence of the nucleon optical potential. We note that for nucleons bound in nuclear matter ($E<0$), the density dependent interaction used in the HF calculations reported in Sec. II were assumed to be independent of energy, i.e., $g(E)=1$ when $E<0$. A more refined treatment would be based upon calculations of the G matrix (using the Paris NN potential) for both positive and negative energies. Unfortunately, these are not currently available.

The density ρ of the two overlapping nuclei which enters Eq. (2.10) is taken to be the sum of the densities of their ground states, evaluated at the midpoint of the internucleon separation,

$$F(\rho)=F\left[\rho_1\left(\mathbf{r}_1+\frac{\mathbf{s}}{2}\right)+\rho_2\left(\mathbf{r}_2-\frac{\mathbf{s}}{2}\right)\right]. \tag{2.11}$$

This is the approximation frequently adopted for calculating folding model potentials [1,23,16,38]. Here, it allows us to use the approximation (2.9) for the mixed density matrices. After certain transformations one obtains the self-consistent and local exchange potential $V_{\rm EX}$ as

$$V_{\rm EX}(E,\mathbf{R})=4\pi g(E)\int_0^\infty v_{\rm EX}(s)j_0(k(\mathbf{R})s/M)s^2ds$$

$$\times\int f_1(\mathbf{r},s)f_2(\mathbf{r}-\mathbf{R},s)F[\rho_1(\mathbf{r})$$

$$+\rho_2(\mathbf{r}-\mathbf{R})]d^3r, \tag{2.12}$$

where

$$f_{1(2)}(\mathbf{r},s)=\rho_{1(2)}(\mathbf{r})\hat{j}_1(k_{F1(2)}(\mathbf{r})s) \quad \text{and} \quad j_0(x)=\sin x/x.$$

The exchange potential (2.12) can then be evaluated exactly by an iterative method [23]. The calculated total potential $V(E,R)$ has a dependence on energy arising from the exchange term which is much stronger than the intrinsic energy dependence represented by the $g(E)$ factor. Consequently, to have a realistic energy dependence for the folded potential, one should treat the knockon exchange effects as accurately as possible. A useful quantity in the study of the energy dependence is the volume integral of the folded potential per interacting nucleon pair

$$J_R(E)/(A_1A_2)=\frac{4\pi}{A_1A_2}\int_0^\infty[V_D(E,r)+V_{\rm EX}(E,r)]r^2dr. \tag{2.13}$$

The ground-state density for the α particle is taken to be a Gaussian form with a rms radius derived from electron-scattering measurements [1], while the densities for the other nuclei considered in our folding calculation are represented by two-parameter Fermi shapes with parameters suggested by shell-model calculations and electron-scattering measurements [38,39]. Since the original M3Y-Paris interaction (2.3)

is real, the simplest approach to obtain a complex optical potential would be to use the density dependent interaction with a complex strength. This would result in the real and imaginary parts of the optical potential having the same shape. However, it is well known from analyses of α-nucleus scattering (for example, see Fig. 2 in Ref. [40]) and of light HI scattering [2,18] that the imaginary potential is definitely required to have a different shape; the ratio of the imaginary to the real potential tends to peak near the nuclear surface but becomes relatively weak in the interior [13] (it is this property which enables us to obtain some knowledge of the real potential at small distances from refractive scattering). Therefore, we have chosen, as in our previous folding analyses, a hybrid (semimicroscopic) approach where the folded potential enters the OM analyses as the real part of the optical potential and the imaginary part is treated phenomenologically, using a conventional Woods-Saxon (WS) form. Thus the total optical potential is

$$U(E,R)=N_R[V_D(E,R)+V_{\rm EX}(E,R)]+iW_V(R)+iW_D(R), \tag{2.14}$$

with

$$W_V(R)=-W_V\left\{1+\exp\left[\frac{R-r_V(A_1^{1/3}+A_2^{1/3})}{a_V}\right]\right\}^{-1} \tag{2.15}$$

and

$$W_D(R)=4W_Da_D\frac{d}{dR}\left\{1+\exp\left[\frac{R-r_D(A_1^{1/3}+A_2^{1/3})}{a_D}\right]\right\}^{-1}. \tag{2.16}$$

The renormalization factor N_R, together with the WS parameters are usually adjusted for the best fit to the data. The WS surface term (2.16) is optional and added only in cases where it essentially improves agreement with the data (in the present paper this is the case for the ^{16}O+^{16}O scattering data). The renormalization factor N_R for the real folded potential is a convenient way to make small adjustments that may be needed to take into account the higher-order (dynamic polarization) contributions to the real potential, as well as taking into account small uncertainties in the folding input that may exist. Consequently, we should find $N_R \simeq 1$ if the procedure is meaningful. The Coulomb potential $V_C(R)$ used in the calculation of the exchange potential [see Eq. (2.8)] and in the OM analysis is generated by folding two uniform charge distributions with radii determined from electron-scattering data for the considered nuclei. All our OM analyses were made using the program PTOLEMY [41].

III. RESULTS AND DISCUSSIONS

A. Systematic folding model analysis of refractive α-nucleus scattering

We have shown in an earlier study [20] that an accurate folding model analysis of refractive α-nucleus scattering, with data measured up to large angles, can be a very effective method to determine the incompressibility of cold nuclear matter. From those analyses [20] (see, for example, results obtained for the $\alpha+^{40}$Ca system at $E_{\rm lab}=104$ MeV shown in Fig. 1) we could determine unambiguously that of the potentials utilized in that study, those derived from the DDM3Y1 and BDM3Y1 interactions were the best choice, thus limiting the predicted value of K to the range between about 170 and 270 MeV.

Now with our hybrid model of the density dependence, which allows a smooth transition between these two interactions (Table I), we aim to determine the optimum K value more precisely by performing a global OM analysis of the available (refractive) α-nucleus elastic scattering on targets ranging from ^{12}C to ^{208}Pb. For this purpose, we have considered elastic $\alpha+^{12}$C scattering data at $E_{\rm lab}=104$ MeV [42], 145 and 172.5 MeV [43]; $\alpha+^{40}$Ca data at 80 MeV [44], 104 MeV [25], and 141.7 MeV [9]; $\alpha+^{58}$Ni data at 104 MeV [45], 139 MeV [8], and 172.5 MeV [46]; $\alpha+^{90}$Zr data at 79.5–118 MeV [47] and at 141.7 MeV [9]; $\alpha+^{208}$Pb data at 104 MeV [48] and 139 MeV [8].

The main feature of these data is that the Fraunhofer diffraction in the forward part of the angular distribution is usually followed by a smooth shoulderlike rainbow maximum which then falls off exponentially at the largest angles [9,13,14]. To illustrate this effect, we have plotted in Fig. 3 the $\alpha+^{58}$Ni, ^{90}Zr, and ^{208}Pb data at a typical ''refractive'' incident energy of 140 MeV, together with the OM fits obtained with the CDM3Y1 and CDM3Y6 folded potentials (see Table II for the parameter values). Although more than two decades have elapsed since these data were measured, they still present some of the best experimental evidence for nuclear rainbow scattering. It was the $\alpha+^{58}$Ni data at 139 MeV that first led one to the importance of density dependence in the folding model analysis (see, e.g., Ref. [16], and references therein). The physics is now well understood [16,20,23,28], namely, the observed refractive (rainbow) pattern in the elastic cross section is due to the α-nucleus optical potential having a relatively weak absorption in the interior. It can be shown from a near- and far-side decomposition of the scattering amplitude [49] that the refractive scattering data are sensitive to the real part of the α-nucleus optical potential down to very small radii. Consequently, these data are of great importance in eliminating the ambiguity in the strength of the real optical potential [9], and to test different theoretical models for the α-nucleus potential. We also note that at small distances, where the α-nucleus overlap density is substantially higher than the normal NM density ρ_0 (see Fig. 4), in-medium effects become stronger and enhance the effects on the potential of the various forms of density dependence. This is illustrated in Fig. 5, which shows the folded potentials for $\alpha+^{40}$Ca at a bombarding energy of 104 MeV. Although when the cross sections are plotted using a logarithmic scale, as in Fig. 1, both the DDM3Y1 and BDM3Y1 interactions appear to give about the same description of the scattering data, the conventional χ-squared value per datum obtained with the BDM3Y1 potential is smaller than that given by the DDM3Y1 potential (Fig. 6).

If the data plotted in Fig. 3 [8,9] are the best evidence for nuclear rainbow scattering observed at a given energy for different targets, high-precision $\alpha+^{90}$Zr data by Put and Paans [47] (see Fig. 7) present a unique picture of how the refractive pattern evolves with energy. While the far-side scattering begins to dominate the large-angle scattering already at the α-particle energy of 60 MeV, the most pro-

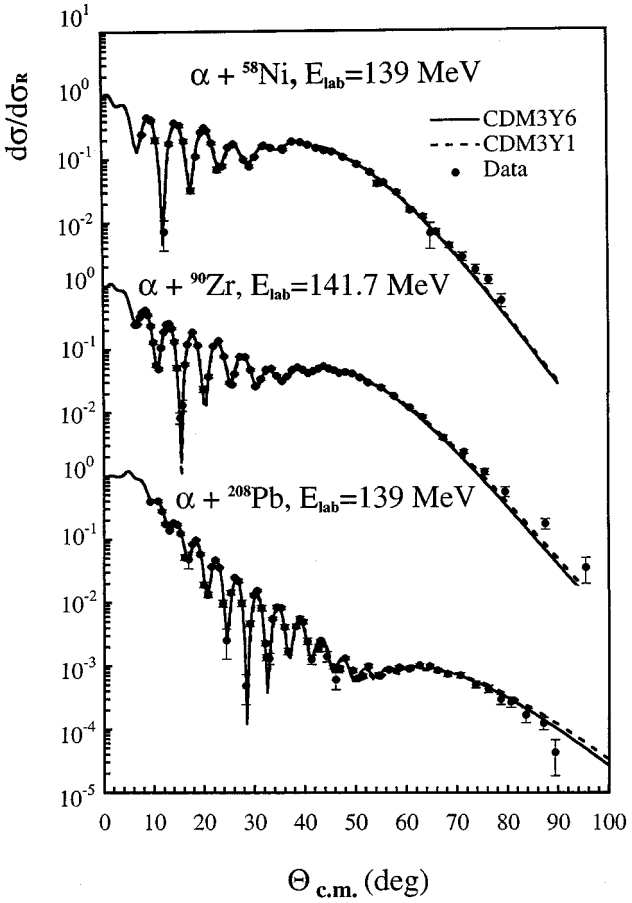

FIG. 3. Fits to the elastic $\alpha+{}^{58}$Ni, ^{90}Zr, and ^{208}Pb scattering data at $E_{\rm lab}\simeq 140$ MeV given by the real folded potentials calculated using the density dependent interactions CDM3Y1 and CDM3Y6 which yield nuclear incompressibilities of $K=188$ and 252 MeV, respectively). The usual Woods-Saxon shape (2.15) was used for the imaginary potentials, and the parameters adjusted to optimize the fits to the data.

nounced rainbow maxima are seen as the energy reaches 80 MeV and higher [20,47]. These data, together with the $\alpha+{}^{90}$Zr elastic data measured at 141.7 MeV [9], provide us with a very accurate test ground for any theoretical model of the $\alpha+{}^{90}$Zr optical potential. In our case, they help to show unambiguously that from the suggested density dependent interactions in Table I the CDM3Y5, CDM3Y6, and BDM3Y1 versions of the density dependent interaction are the most favored ones (see the lower part of Fig. 8).

From the detailed OM analyses of the other α scattering data, we find indeed a systematic behavior of the χ^2 value to approach its minimum with the CDM3Y5, CDM3Y6, or BDM3Y1 interactions (see Figs. 6, 8, and 9). These three types of the density dependent interaction, in a HF calculation of cold NM, give the nuclear incompressibility to be $K=241$, 252, and 270 MeV, respectively. This is a strong indication that a very soft nuclear EOS (with K around 180 MeV, such as is often used in calculations of supernova explosions) is less realistic than a slightly stiffer EOS (with $K\simeq 240-270$ MeV).

We note that there is some preference (especially in some nuclear structure calculations) for an interaction whose density dependence is somewhat softer than the linear density dependence of the BDM3Y1 version, such as is given by the CDM3Yn ($n=3\rightarrow 6$) examples studied here. The CDM3Y3 and CDM 3Y4 versions, e.g., are very close to what one would get from using the power-law dependence (1.3) with a popular choice [24] for the noninteger power, $\beta=2/3$ (which gives $K=218$ MeV [22]), although we avoided using it explicitly because of computational problems when it is applied to calculations of folding model potentials. We also note that even with $K=270$ MeV, we are still dealing with quite a soft EOS compared with the *hard* EOS sometimes considered in the study of HI collisions (with $K\simeq 400-500$ MeV) [31].

It is well known that frequently there is an interplay between the real and imaginary parts of the optical potential in an OM analysis of elastic scattering. In our folding analysis of the α-nucleus scattering, we have allowed a renormalization of the real folded potential (2.5) as well as adjusting the parameters of the imaginary WS optical potential to give the best fit to the data in each particular case (see, for example, the OM parameters used with the CDM3Y6 folded potential in Table II); and the effects of using the different real folded potentials (Fig. 5, for example) are somewhat obscured by adjusting the N_R coefficient and the parameters of the WS imaginary potential. Nonetheless, there does seem to be clear evidence from refractive α scattering on targets ranging from ^{12}C to ^{208}Pb that favors a value of K closer to that given by BDM3Y1 than that resulting from DDM3Y1, as well as a definite preference in many cases for K in the range of about 240 to 270 MeV.

The OM parameters obtained with the types of folded potential other than CDM3Y6 are very close to those obtained with the CDM3Y6 potential itself and given in Table II. We regard these CDM3Y6 parameters as representative of a ''realistic'' potential for use in a folding model analysis of α scattering (we note that the optimum values of N_R are greater than unity, between 1.2 and 1.3. This has been seen as a characteristic of folding models for α scattering [16,17,20,50], but no satisfactory explanation has yet been offered). As in other OM analyses of the same data, we find that the best-fit imaginary WS potentials are quite shallow relative to the real potentials, confirming the relatively weak absorption experienced in the scattering which in turn helps us to trace differences in the real folded potentials at small radii. It is remarkable that different OM analyses of the same α-nucleus (refractive) scattering data considered here, using various forms of the optical potential such as Woods-Saxon squared potentials [8,9], spline funtions [47] or those from model-independent analyses (MIA) [27,50], have always resulted in a shallow imaginary potential and a deep (folding-like) real potential. Compared to the HI scattering, the α-nucleus optical potential has almost no ''family'' problem (the existence of different families of the optical potential which give the same fit to the data), especially when the systematic behavior of the volume integrals of the optical potential is involved in the study [50]. Our results for the volume integral (2.13) of the real folded potential per interacting nucleon pair (obtained with the CDM3Y6 interaction) are shown in Table II. They are in very close agreement with the systematics given by other OM analyses (see, e.g., Ref. [50]).

TABLE II. OM parameters [see Eqs. (2.14) and (2.15)] used in the folding analysis of elastic α scattering on different targets. The real folded potentials were calculated using the CDM3Y6 interaction which yields the nuclear incompressibility $K=252$ MeV (see Table I).

Target	$E_{\rm lab}$ (MeV)	N_R	$-J_R/4A$ (MeV fm^3)	$\langle r_R^2\rangle^{1/2}$ (fm)	W_V (MeV)	r_V (fm)	a_V (fm)	σ_R (mb)	χ^2
^{12}C	104	1.271	319.3	3.386	18.36	0.959	0.621	788	10.6
	145	1.287	300.3	3.401	18.59	0.969	0.667	781	2.4
	172.5	1.249	277.3	3.411	20.54	0.910	0.718	747	3.5
^{40}Ca	80	1.201	322.1	4.279	21.31	1.051	0.771	1554	3.3
	104	1.192	306.0	4.284	20.62	1.079	0.727	1511	4.5
	141.7	1.177	282.1	4.292	20.03	1.071	0.687	1411	7.0
^{58}Ni	104	1.160	286.3	4.555	19.46	1.116	0.610	1629	10.4
	139	1.151	266.6	4.562	21.19	1.063	0.737	1664	2.4
	172.5	1.151	251.0	4.568	25.88	0.996	0.811	1650	3.9
^{90}Zr	79.5	1.191	306.8	5.037	19.03	1.135	0.614	1931	4.8
	99.5	1.191	295.9	5.040	19.63	1.136	0.620	1968	4.7
	118	1.170	281.0	5.043	19.67	1.131	0.654	1998	2.1
	141.7	1.155	265.7	5.046	20.63	1.107	0.704	2011	4.1
^{208}Pb	104	1.354	335.2	6.268	32.69	1.103	0.781	2935	8.1
	139	1.174	272.8	6.271	20.34	1.165	0.722	2952	5.9

Thus the weak absorption observed in α-nucleus scattering at these energies that lead to the appearance of rainbow-like features in the dominant far-side scattering amplitude at large angles offers a unique opportunity to study the density dependence of an in-medium NN interaction. Such a density dependence is well understood and predicted in many G-matrix calculations. Another crucial point in this connection is the usefulness of the very high and compact density profile of the α particle. One has a density as high as $\rho\simeq 2\rho_0$ in the center of the ^{4}He nucleus, given by the Gaussian distribution (see Fig. 4) used in our folding analysis as well as by the empirical matter density (given by twice the experimental charge density for ^{4}He [51] with the finite-sized charge distribution of the proton unfolded). This means that the total density for an α particle overlapping a target nucleus may reach as much as $3\rho_0$. From Fig. 4 one can see that for the $\alpha+^{40}$Ca system the overlap density begins to approach $3\rho_0$ already at a separation of $R=4$ fm. The real optical potential can be very well determined at such a radius if the bombarding energy is sufficiently high.

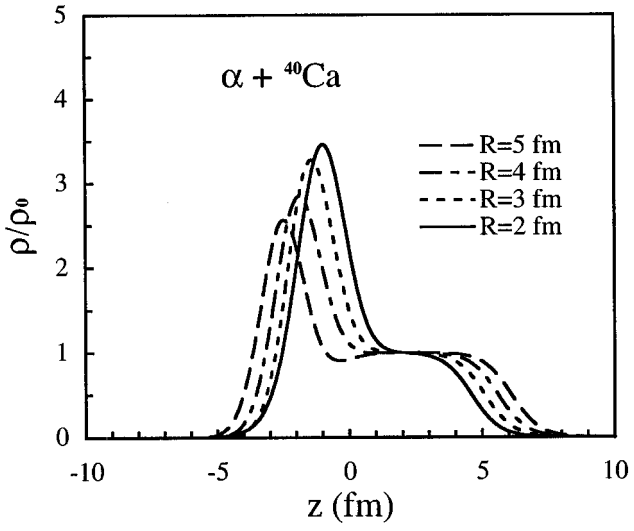

FIG. 4. Overlap density of the $\alpha+^{40}$Ca system at different internuclear distances. The z axis is directed along the line connecting the centers of the two nuclei.

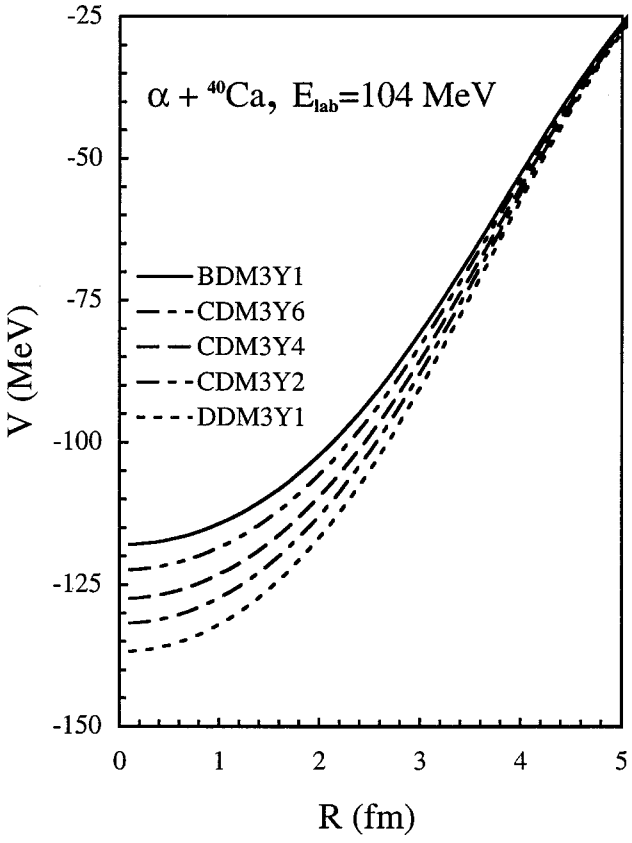

FIG. 5. Radial shapes of different folded potentials for the $\alpha+^{40}$Ca system at $E_{\rm lab}=104$ MeV which were calculated using the various density dependent M3Y-Paris interactions of Table I.

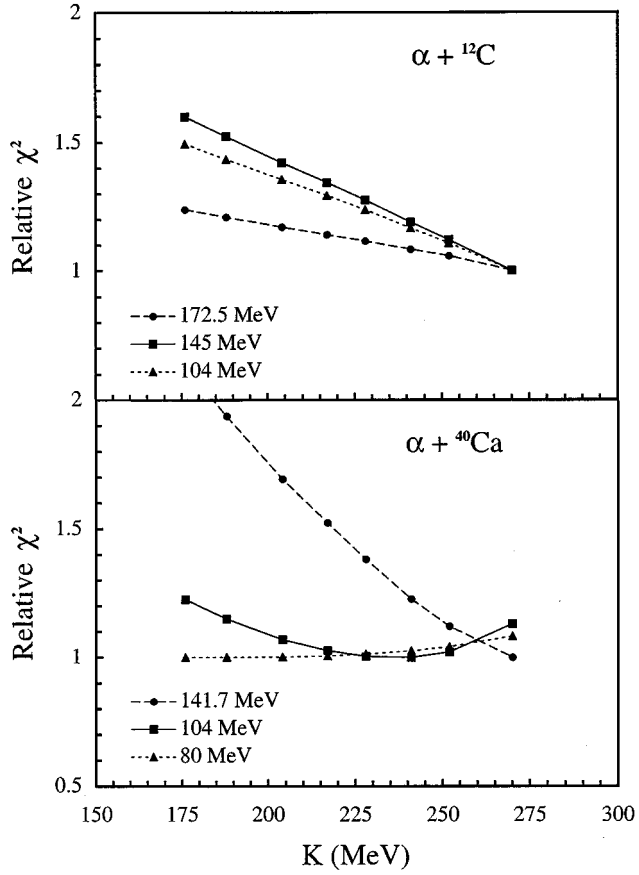

FIG. 6. Relative χ^2 values (in ratio to the lowest χ^2 value obtained in each case) of the OM fits to the elastic data for $\alpha+{}^{12}$C and ^{40}Ca, versus the corresponding (discrete) K values given by the different density dependent M3Y-Paris interactions (see Table I), which were used to generate the real folded potentials. The lines are only to guide the eye.

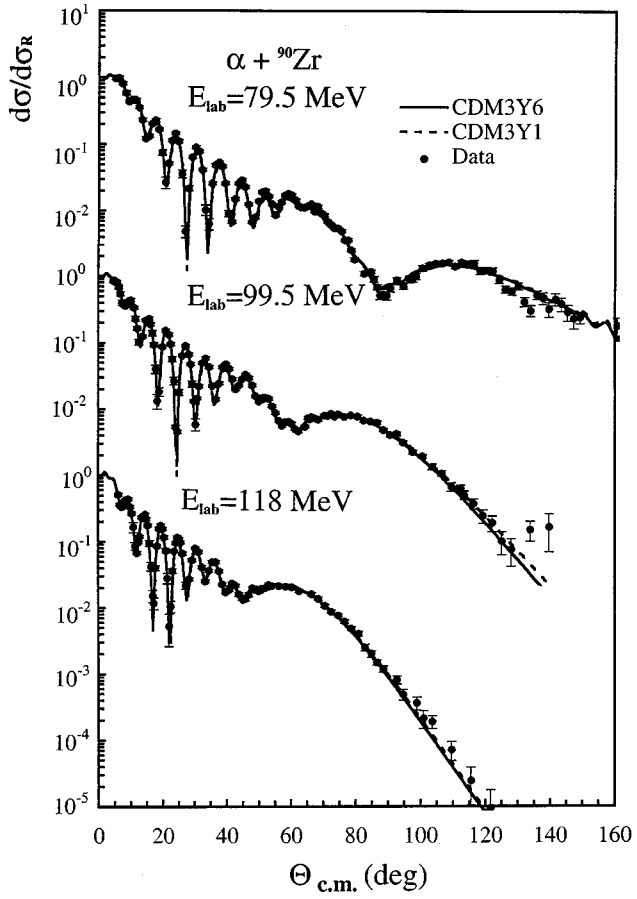

FIG. 7. The same as Fig. 3 but for the $\alpha+{}^{90}$Zr system at $E_{\rm lab}=79.5$, 99.5, and 118 MeV.

It is also conceivable that the appearance of such abnormally high overlap densities is related to the problem just noted that the renormalization factor N_R is found to be greater than unity. The density dependences considered here were not designed to cover such large departures from normal NM density and may become deficient at such high densities.

B. Folding analysis of refractive ^{12}C and ^{16}O elastic scattering

In contrast to α-nucleus scattering, the elastic scattering of heavier ions is usually of peripheral character. The far-side elastic scattering pattern at large angles is usually suppressed by strong absorption, and the Fraunhoffer diffractive pattern in the angular distribution at smaller angles that is observed for many HI systems can be reproduced by many optical potentials which all have similar values and similar slopes near the so-called strong absorption radius [1]. It then becomes more difficult to test the reliability of theoretical models which have been used to generate the potentials.

Nevertheless, the elastic scattering for some light HI systems, like ^{12}C+^{12}C and ^{16}O+^{16}O, has been shown to display prominent refractive patterns at energies from 15 to 100 MeV/nucleon [2,10–12,21,52]. Despite uncertainties in some particular cases, systematic OM analyses [2,13,53] of most of the available data have indicated that a family of deep (namely, depths ranging from about 100 to 300 MeV) real optical potentials, associated with quite shallow imaginary potentials, are required to explain the rainbow features observed in experiments. Our recent folding analyses of those data [21,23] have shown clearly that the real folded potential and the best-fit WS imaginary potential obtained therewith also belong to this family. Like the folding analysis of the α-nucleus scattering [20], the results obtained for light HI (refractive) scattering [21,23] have also unambiguously suggested the DDM3Y1 and BDM3Y1 interactions to be the most realistic versions of the density dependent M3Y interaction. Thus it is also of interest to test new density dependent forms developed in the present work against the same light HI scattering data.

Before discussing the results of the OM analyses, we would like to point out some differences in the overlap densities which occur in a collision between two heavy ions compared with those for a typical α-nucleus case. In Fig. 10 we show the sum of the two densities for a ^{16}O+^{16}O collision, at various internuclear distances R, expressed as a function of the distance z from their center of mass. One finds that the highest overlap density that can be reached in this system is about $2\rho_0$, and that only occurs when R is less than about 3 fm. In the $\alpha+{}^{40}$Ca system, the overlap density begins to approach $3\rho_0$ already at $R\simeq 4$ fm (see Fig. 4). This difference (caused by the much higher density profile of the α particle) also leads to a different picture of the folded potentials obtained for these two cases. For example, the

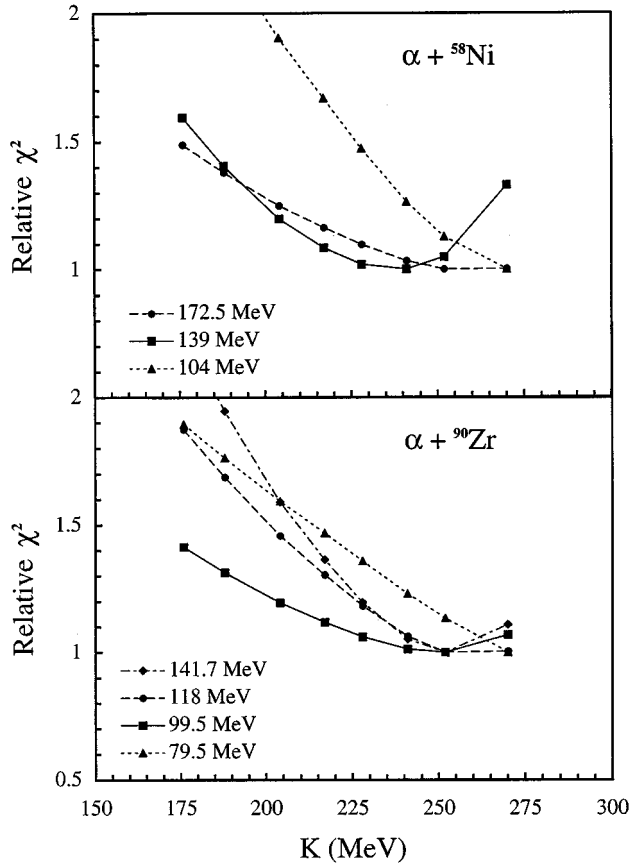

FIG. 8. The same as Fig. 6 but for the $\alpha+{}^{58}$Ni and ^{90}Zr systems.

DDM3Y1 and BDM3Y1 potentials calculated for the $\alpha+{}^{40}$Ca system at 104 MeV have a relative difference of about 16% at smallest R (Fig. 5), and this change has been shown to affect the elastic scattering (Fig. 6). However, for the ^{16}O+^{16}O system at 350 MeV, the difference between these two types of the folded potential (Fig. 11) is only about 5%. This has much less effect on the elastic scattering, and thus it becomes much harder to trace differences in the folded potentials through OM analyses. In particular, such small changes can easily be obscured by the use of the renormalization factor N_R for the folded potential.

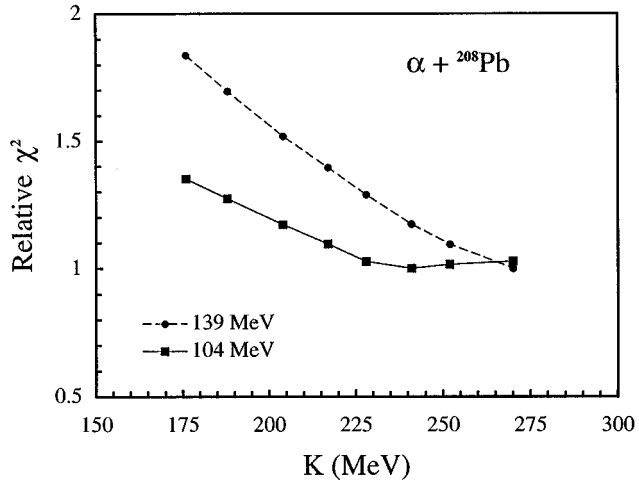

FIG. 9. The same as Fig. 6 but for the $\alpha+{}^{208}$Pb system.

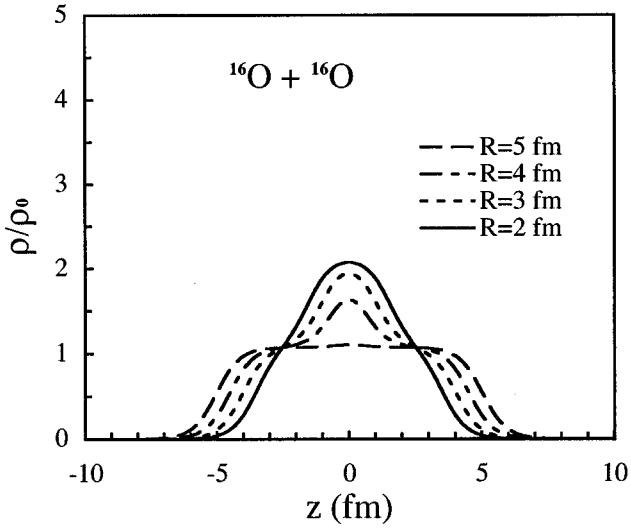

FIG. 10. The same as Fig. 4 but for the ^{16}O+^{16}O system.

The ^{12}C+^{12}C system is one of the most intensely studied light HI systems, with scattering data measured at incident energies ranging from a few up to 200 MeV/nucleon. Very interesting are the low-energy data measured by Stokstad *et al.* [54] where the optical potentials have been shown [53,54] to be surprisingly transparent and the data can provide some information on the ^{12}C+^{12}C potential in the interior. In the present work we have performed the folding analyses for the ^{12}C+^{12}C data at $E_{\rm lab}=112$ and 126.7 MeV [54] and found indeed a very weakly absorbing optical potential for these low-energy data (see Table III). We have also analyzed the elastic data for this system measured at 240 and 300 MeV [10,11], where a rainbow enhancement of the scattering cross section at large angles has been observed (see lower part of Fig. 12). In addition, we have analyzed several data sets at higher energies, namely, the elastic ^{12}C+^{12}C data at 1016 MeV [55], ^{16}O+^{12}C data at 608 MeV [56], and 1503 MeV [57]. The newly measured ^{16}O+^{12}C data at 129 MeV [58] has also been studied.

All the results show that the folded potentials obtained with the CDM3Y*n* set of density dependent interactions (Table I) give about the same good fit to the data when judged ''by eye'' (see Figs. 12 and 13). This indicates that they belong to the same overall ''family'' of realistic optical potentials. In contrast to the α scattering considered above, the χ^2 values obtained for light HI systems (Fig. 14) do not show any marked variation with the theoretical K value. While the results obtained for ^{12}C+^{12}C at 112 and 126.7 MeV, and ^{16}O+^{12}C at 1503 MeV seem to favor the CDM3Y6 and BDM3Y1 interactions, those from the analyses of the data for ^{12}C+^{12}C at 240, 300, and 1016 MeV seem to show a reverse trend (Fig. 14). Given that the maximum overlap density reached in a light HI system is smaller than that of an α-nucleus system, as well as the measurements being less extensive than those obtained for the α-nucleus cases, the results shown in Fig. 14 only indicate that the heavy ion data are less sensitive to the small differences in the folded potentials caused by the various density dependences. The sensitivity is further obscured by the freedom we have to allow the renormalization factors N_R for the real folded potentials to deviate slightly from unity.

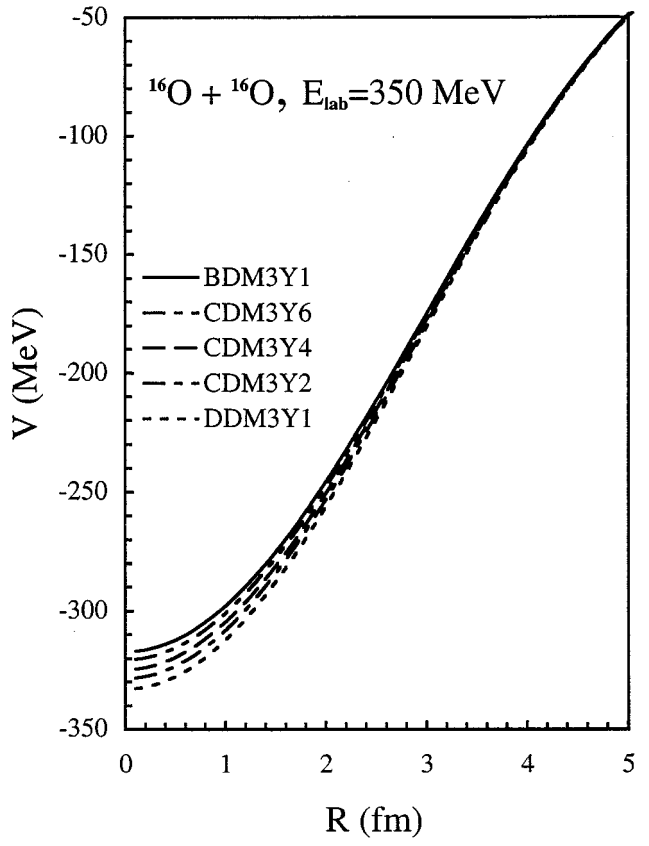

FIG. 11. The same as Fig. 5 but for the ^{16}O+^{16}O system at $E_{\rm lab}=350$ MeV.

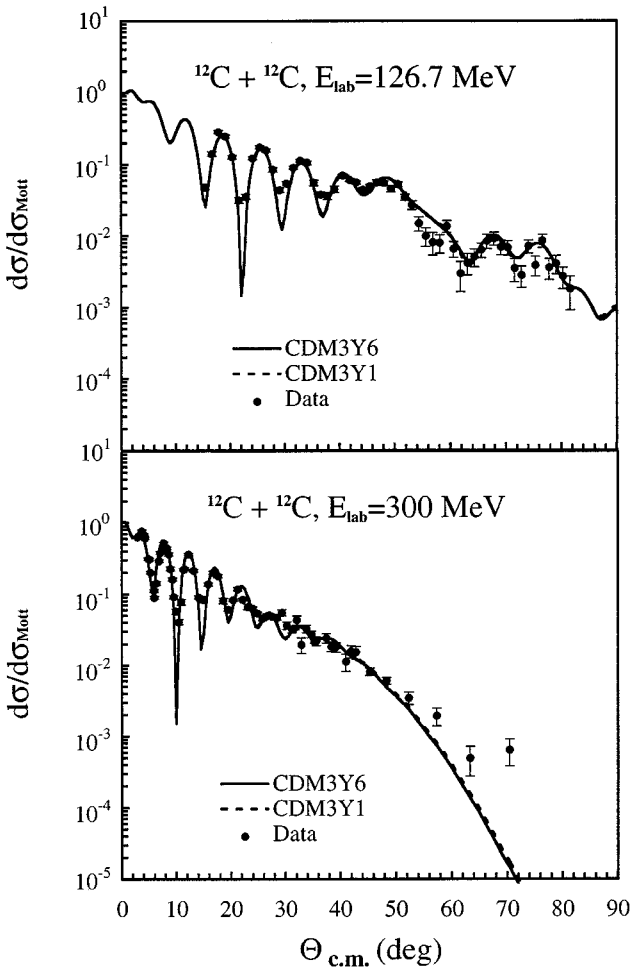

FIG. 12. The same as Fig. 3 but for the ^{12}C+^{12}C system at $E_{\rm lab}=126.7$ (upper part) and 300 MeV (lower part).

We note that these same data have been used quite successfully to differentiate between different density dependent interactions when those yield K values that differ from each other by about 100 MeV or more [21,23]. Among these data

TABLE III. OM parameters [see Eqs. (2.14), (2.15), and (2.16)] used in the folding analysis of elastic ^{12}C and ^{16}O scattering. The real folded potentials were calculated using the CDM3Y6 interaction which yields the nuclear incompressibility $K=252$ MeV (see Table I).

System	$E_{\rm lab}$ (MeV)	N_R	$-J_R/(A_1A_2)$ (MeV fm^3)	$\langle r_R^2\rangle^{1/2}$ (fm)	W_V (MeV)	r_V (fm)	a_V (fm)	σ_R (mb)	χ^2
^{12}C+^{12}C	112	0.997	339.2	3.819	17.67 [a]	1.156	0.627	1382	12.8
	126.7	0.983	331.1	3.820	17.91 [a]	1.180	0.571	1355	8.8
	240	0.912	285.9	3.830	26.84 [a]	1.126	0.657	1426	11.3 [e]
	300	0.885	267.2	3.835	26.17 [a]	1.123	0.665	1398	11.3 [e]
	1016	0.897	172.9	3.908	18.28 [a]	1.088	0.825	1182	14.8
^{16}O+^{12}C	129	1.061	375.7	3.998	20.09 [a]	1.225	0.579	1575	22.9 [e]
	608	0.804	226.6	4.027	25.04 [a]	1.110	0.607	1346	6.7
	1503	0.850	156.5	4.093	17.33 [a]	1.144	0.778	1307	13.0
^{16}O+^{16}O	250	0.859	295.8	4.178	41.51 [b]	0.867	0.957	1822	8.0 [e]
	350	0.909	298.3	4.184	24.63 [c]	1.148	0.638	1632	4.8 [e]
	480	0.829	255.7	4.191	31.16 [d]	1.067	0.749	1649	5.2 [e]

[a]No surface term in the imaginary WS potential, i.e., $W_D=0$.
[b]$W_D=5.141$ MeV, $r_D=1.131$ fm, $a_D=0.479$ fm.
[c]$W_D=8.52$ MeV, $r_D=0.933$ fm, $a_D=0.362$ fm.
[d]$W_D=1.84$ MeV, $r_D=0.971$ fm, $a_D=0.217$ fm.
[e]χ^2 values obtained with uniform 10% errors.

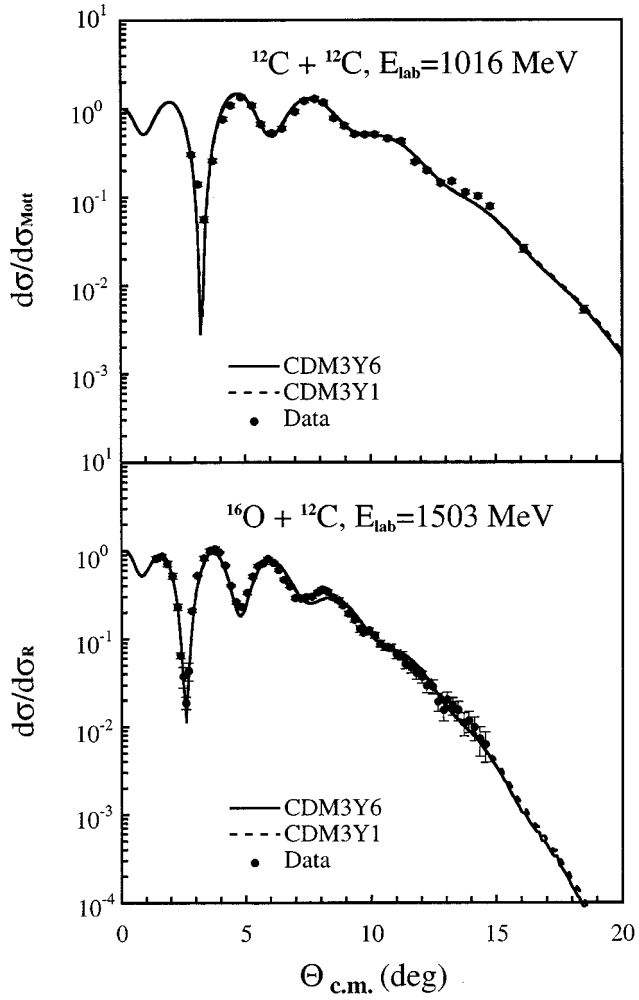

FIG. 13. The same as Fig. 3 but for the ^{12}C+^{12}C system at E_{lab}=1016 MeV (upper part) and ^{16}O+^{12}C system at E_{lab}=1503 MeV (lower part).

sets, the ^{16}O+^{12}C elastic data at 1503 MeV are somewhat more complete (lower part of Fig. 13). They have been shown by Kobos *et al.* [59] to be sensitive to the real optical potential at distances R from 3 to 6 fm. That gives us some reason to emphasize the χ^2 behavior found in this case, which favors the use of the BDM3Y1 interaction and supports the conclusion drawn from the study of α-nucleus scattering in Sec. III A.

Among light HI systems, the ^{16}O+^{16}O elastic data measured at HMI-Berlin [12,21,52] are the most extensive and exhibit refractive scattering most clearly. For example, the broad maximum near 50° in the data at 350 MeV (lower part of Fig. 15) can be identified as a remnant of the primary rainbow, with the first Airy minimum around 44°. This rainbow structure can be reproduced if the real optical potential is deep enough to belong to the group of refractive potentials [23]. These very accurate data, covering almost the whole allowed angular range (symmetry about 90° being required), have allowed one to perform model independent analyses of the data [52,60], and to test the sensitivity to the ^{16}O+^{16}O potential at radii as small as 3 fm. Results of a folding analysis of these data using the new density dependent interactions are shown in Figs. 15 and 16. Again, judged visually, good fits are obtained with all the folded potentials considered

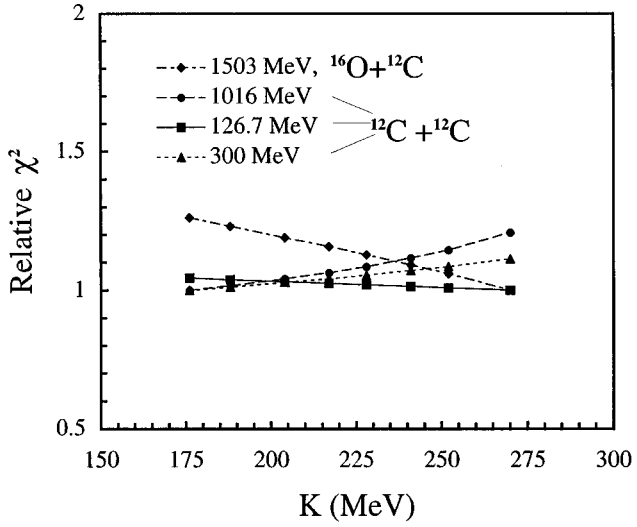

FIG. 14. The same as Fig. 6 but for the ^{12}C+^{12}C system at E_{lab}=126.7, 300, and 1016 MeV, and ^{16}O+^{12}C system at E_{lab}=1503 MeV.

here. Even the χ^2 values obtained (upper part of Fig. 17) show almost no variation with the kind of density dependence chosen. The reason is quite clear: a small difference of about 5% in the depth of the potential at the smallest radii (see Fig. 11) is too small to be traced in the OM analysis.

Encouraged by the success of the MIA analysis of the ^{16}O+^{16}O elastic data considered here [52], we try to avoid the traditional renormalization procedure in the folding analysis by treating explicitly the real part of the dynamic polarization potential (DPP). This DPP represents other contributions to the Feshbach optical potential, including those which lead to absorption from the elastic channel and thus give rise to the imaginary part of the potential. The overall success of the folding model implies that the real part of the DPP contributes a relatively small part to the real optical potential. The sign of this real contribution is expected to depend upon the physical processes involved [4]. Coupling to breakup channels tends to result in a repulsive DPP, whereas the excitation of collective surface oscillations tends to induce an attractive DPP [49]. Both effects are usually located in the surface region. When simply renormalizing the folded potentials we have found (with one exception) that $N_R<1$ (see Table III) was required. However, we should not immediately assume that this implies that breakup is the source of the DPP; small departures of N_R from unity may be taking account other uncertainties in the construction of the folded potentials, including other exchanges beyond the Fock term in Eq. (2.5). In principle the DPP can be estimated by a full coupled-channel reaction calculation [4]. In practice, this is not easy. However, with the highly accurate and extensive data available, we try to represent the DPP in our folding analysis by adding a real surface correction term $\Delta V(R)$ to the folded potential. The optical potential then becomes

$$U(E,R)=V_D(E,R)+V_{EX}(E,R)+\Delta V(R)+iW_V(R)+iW_D(R), \tag{3.1}$$

where the shape of $\Delta V(R)$ is defined by its values at certain

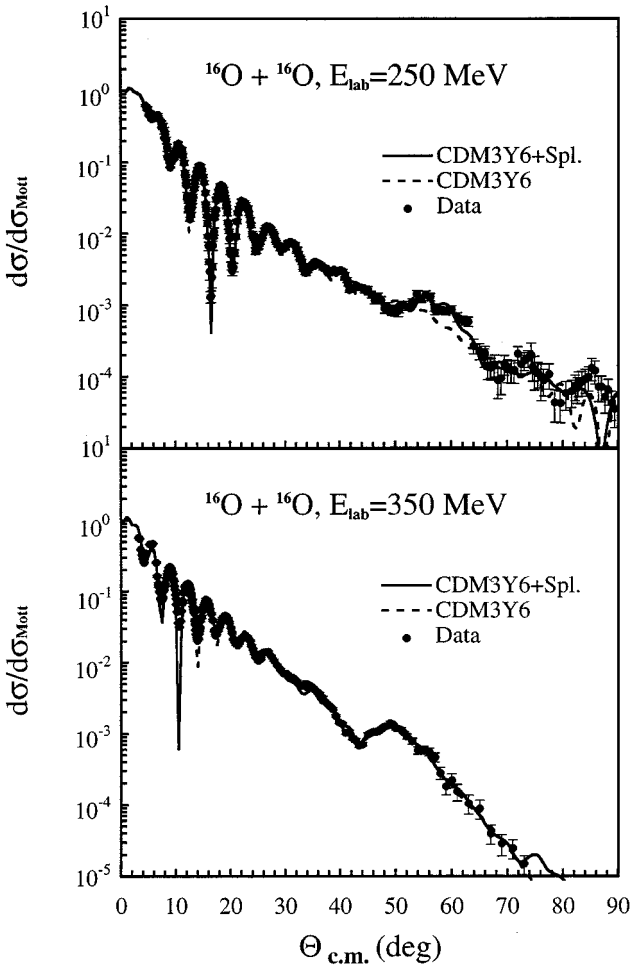

FIG. 15. Fits to the elastic ^{16}O+^{16}O scattering data at $E_{\rm lab}$=250 and 350 MeV given by OM analyses using renormalized real folded potentials (dashed curves) and real ''folded+spline'' potential (unrenormalized, N_R=1) (solid curves). The imaginary potentials were taken to have the Woods-Saxon (volume+surface) shape [see Eqs. (2.14), (2.15), and (2.16)]. The parameters of the optical potentials are given in Tables III and IV.

radial knots with a cubic spline interpolation between the knots. The $\Delta V(R)$ values at the knots are parameters adjusted to fit the scattering data and no renormalization of the main folded potential is assumed in these calculations. That is, we take N_R=1. Although in such a folding+spline analysis there are more free parameters, we may hope for the results to be more significant than those obtained simply by renormalizing the folded potential as a whole. We note that such a folding+spline procedure has been used successfully to reveal the contribution to the real part of the DPP from the breakup effect in our recent study of ^{6}Li+^{12}C elastic scattering [61]. Given that we expect the real DPP to be strongest in the surface region, the DPP correction $\Delta V(R)$ was defined for the radial range $2 \leqslant R \leqslant 10$ fm only, with its value at R=2 fm set equal to zero. The values at the seven radial knots R=3(1)10 fm, as well as the parameters of the imaginary potential, were varied to optimize the fit to the data. We expected that the most physical one of the set of folded potentials would be that one which gave the lowest χ^2 in such a procedure.

The results of this folding+spline analysis are shown as

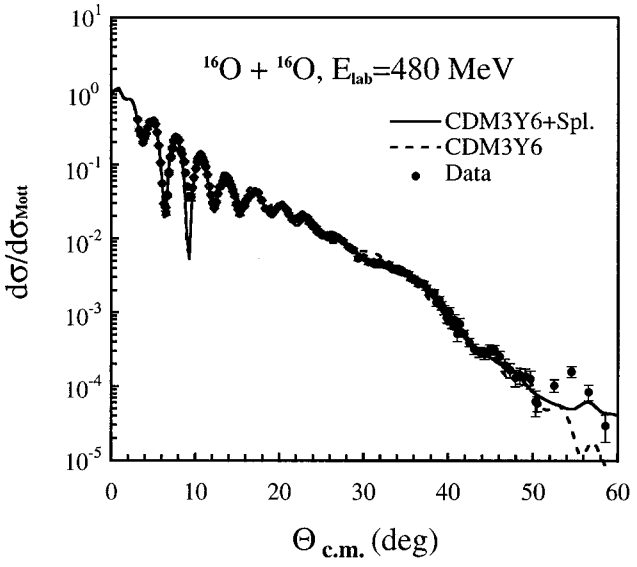

FIG. 16. The same as Fig. 15 but for the ^{16}O+^{16}O system at $E_{\rm lab}$=480 MeV.

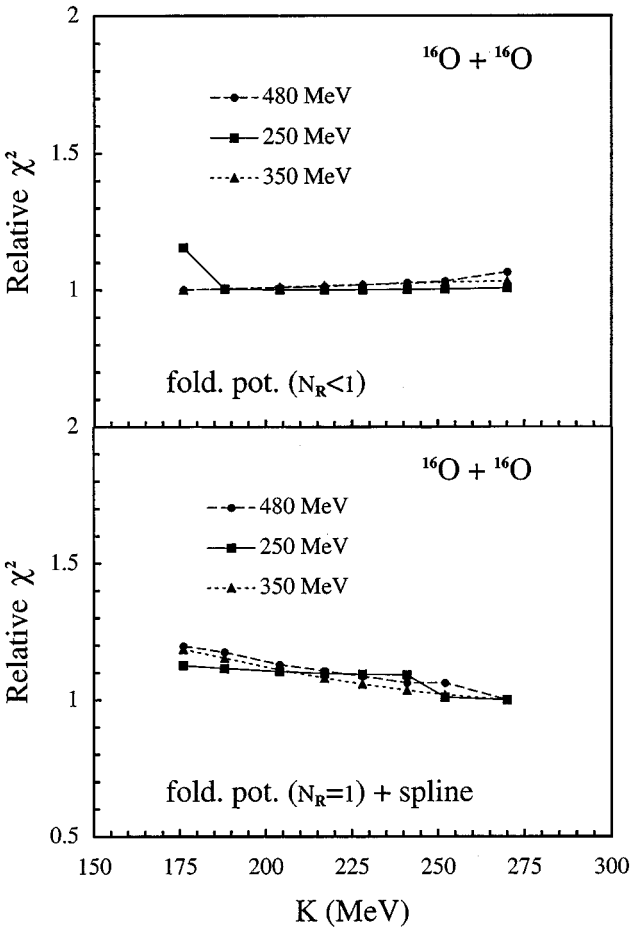

FIG. 17. The same as Fig. 6 but for the ^{16}O+^{16}O system at $E_{\rm lab}$=250, 350, and 480 MeV. The upper part shows the χ^2 values obtained by renormalizing the folded potentials, while the lower part shows the χ^2 obtained by adding the spline correction to the unrenormalized folded potentials.

TABLE IV. Optical potential used in the folding+spline analysis of elastic $^{16}O+^{16}O$ scattering. Imaginary potential was taken in a Woods-Saxon (volume+surface) form [see Eqs. (2.15) and (2.16)] and real potential taken as $V+\Delta V$. The folded potential V was calculated using the CDM3Y6 interaction (see Table I), and the surface correction (added to V at $R=3-9$ fm) ΔV was given by a spline fit. No renormalization was assumed for V, i.e., $N_R=1$.

$E_{\rm lab}$ (MeV)	W_V (MeV)	r_V (fm)	a_V (fm)	W_D (MeV)	r_D (fm)	a_D (fm)	σ_R (mb)	χ^2
250	29.48	1.0	0.975	4.602	1.007	0.334	1925	4.3 [a]
350	23.88	1.182	0.542	9.725	1.021	0.291	1574	3.8 [a]
480	27.52	1.024	0.443	9.204	1.024	0.727	1601	3.6 [a]
$E_{\rm lab}$ (MeV)	R (fm)	3	4	5	6	7	8	9
250	$V+\Delta V$ (MeV)	−138.7	−94.2	−38.5	−14.7	−4.0	−0.70	−0.03
	ΔV (MeV)	45.8	15.0	12.8	3.9	1.3	0.54	0.21
350	$V+\Delta V$ (MeV)	−141.7	−99.8	−51.6	−16.5	−5.1	−1.28	−0.15
	ΔV (MeV)	34.3	4.4	−2.5	1.4	0.01	−0.08	0.09
480	$V+\Delta V$ (MeV)	−137.5	−90.8	−41.7	−14.1	−4.0	−0.95	−0.12
	ΔV (MeV)	28.0	7.1	4.6	3.0	1.0	0.20	0.11

[a] χ^2 values obtained with uniform 10% errors.

solid curves in Figs. 15 and 16, while the results of simply renormalizing the folded potential without any spline correction are shown as the dashed curves. The use of the spline correction shows a slightly better agreement with the data at the largest angles. The χ^2 values obtained with the splines are shown in the lower part of Fig. 17 and they show clearly that the minimum in χ^2 is reached with the CDM3Y6 or BDM3Y1 versions of the density dependent interaction, although the gain is rather small for the reasons discussed above. This result is in agreement with our much less ambiguous findings from the analyses of the refractive α scattering data (Figs. 6 and 8).

The optical potential parameters found with the CDM3Y6 interaction in our folding+spline analysis of the $^{16}O+^{16}O$ data at 250, 350, and 480 MeV are given in Table IV. Also given explicitly are the values of the real potential at the most important radial knots. We see that the spline correction is by no means negligible, and is generally repulsive (hence the need for a renormalization N_R of less than unity when the splines are not used). Table IV shows that the χ^2 has been reduced at each energy compared to that obtained by simply renormalizing the folded potential (Table III). We do not claim that these potentials are unique, but we believe that they can serve as a useful reference point for any future analyses of these interesting measurements.

IV. SUMMARY

We have introduced some generalized and realistic explicit density dependences into the original M3Y effective NN interactions that were based upon the G-matrix elements of the Paris NN potentials [7]. The values of the parameters that describe the density dependence have been chosen so as to reproduce the saturation properties (binding energy and saturation density) of normal nuclear matter within a Hartree-Fock scheme, and which predict the nuclear incompressibility K to have values ranging from 176 to 270 MeV, in steps of about 10 MeV. Although the functional form of the density dependence was chosen to facilitate folding calculations of nucleus-nucleus potentials, it can also be used as an effective interaction in a nuclear structure model.

The density dependent interactions have been used in the double-folding model to calculate the real parts of α-nucleus and heavy-ion optical potentials for those systems where strong refractive scattering patterns have been observed. In this way we use optical model analyses to probe the sensitivity of the scattering data to different forms of the density dependence and hence to the various values of the associated incompressibility K of cold nuclear matter.

From the detailed OM analyses of elastic α scattering data on targets ranging from ^{12}C to ^{208}Pb, we found a systematic behavior of the χ^2 value per datum to approach its minimum when the real optical potentials are generated by those versions of the density dependent interaction which yield $K=241$, 252, and 270 MeV. We regard this as a strong indication that a very soft nuclear EOS (with K around 180 MeV) is less realistic than one with a slightly stiffer EOS (with $K\simeq 240-270$ MeV).

Analogous folding analyses have been done on elastic-scattering data for $^{12}C+^{12}C$, $^{16}O+^{12}C$, and $^{16}O+^{16}O$ at incident energies up to 94 MeV/nucleon. The results were found to be much less sensitive, but are compatible with those found for α scattering. This lack of sensitivity is due mainly to the maximum overlap density formed in a HI system being appreciably less than that formed in an α-nucleus sytem. This makes much smaller the differences between the potentials calculated using the various density dependences (compare Figs. 5 and 11). In an attempt to trace such a fine effect, we have performed some OM analysis of the new and extensive $^{16}O+^{16}O$ data measured at several energies. For this we used the unrenormalized folded potential, together with a correction term constructed from splines to represent, for example, an explicit contribution from the dynamic polarization potential. This replaces the freedom of using a renormalization factor N_R that differs from unity. The results of this ''folding+spline'' analysis improve the fits somewhat, and show a tendency to favor the same density dependences that were favored in the OM analyses of the α-nucleus scattering.

Thus, the results obtained allow us to claim that a realistic K value is confined to a range of about 240–270 MeV, ruling out the lower value of about 180 MeV indicated as possible

by our original analysis. This still corresponds to a moderately ''soft'' nuclear equation of state. It also allows us to suggest which is the most realistic density dependent interaction which is currently available for folding-model calculations of α-nucleus and nucleus-nucleus potentials. In particular, our results show clearly the importance of refractive α scattering experiments as a means to provide accurate data to test an effective NN interaction.

ACKNOWLEDGMENTS

We thank H.G. Bohlen, H.J. Gils, and A.A. Ogloblin for helpful communications on the tabulated scattering data. Considerable help by C.L. Wu in handling the graphics software is much appreciated. We are also indebted to A. Mezzacappa for helpful comments on the role of the NM compression modulus in supernovas explosions. Nuclear physics research at Chung Yuan Christian University is supported by the National Science Council of the Republic of China. Theoretical nuclear physics research at the University of Tennessee is supported by the U.S. Department of Energy through Contract Nos. DE-FG05-93ER40770 and DE-FG05-87ER40461. Oak Ridge National Laboratory is managed by Lockheed Martin Energy Research Corporation for the U.S. Department of Energy under Contract No. DE-AC05-96OR22464.

[1] G. R. Satchler and W. G. Love, Phys. Rep. **55**, 183 (1979).
[2] M.-E. Brandan and G. R. Satchler, Phys. Rep. (in press).
[3] H. Feshbach, *Theoretical Nuclear Physics* (Wiley, New York, 1992).
[4] Y. Sakuragi, Phys. Rev. C **35**, 2161 (1987); Y. Sakuragi, M. Yahiro, and M. Kamimura, Prog. Theor. Phys. Suppl. **89**, 136 (1986).
[5] G. R. Satchler, Phys. Rep. **91**, 147 (1991).
[6] G. Bertsch, J. Borysowicz, H. McManus, and W. G. Love, Nucl. Phys. **A284**, 399 (1977).
[7] N. Anantaraman, H. Toki, and G. F. Bertsch, Nucl. Phys. **A398**, 269 (1983).
[8] D. A. Goldberg, S. M. Smith, H. G. Pugh, P. G. Roos, and N. S. Waal, Phys. Rev. C **7**, 1938 (1973).
[9] D. A. Goldberg, S. M. Smith, and G. F. Burdzik, Phys. Rev. C **10**, 1362 (1974).
[10] H. G. Bohlen, M. R. Clover, G. Ingold, H. Lettau, and W. von Oertzen, Z. Phys. A **308**, 121 (1982).
[11] H. G. Bohlen, X. S. Chen, J. G. Cramer, P. Fröbrich, B. Gebauer, H. Lettau, A. Miczaika, W. von Oertzen, R. Ulrich, and Th. Wilpert, Z. Phys. A **322**, 241 (1985).
[12] E. Stiliaris, H. G. Bohlen, P. Fröbrich, B. Gebauer, D. Kolbert, W. von Oertzen, M. Wilpert, and Th. Wilpert, Phys. Lett. B **223**, 291 (1989).
[13] M. E. Brandan and K. W. McVoy, Phys. Rev. C **55**, 1353 (1997).
[14] M. E. Brandan, M. S. Hussein, K. W. McVoy, and G. R. Satchler, Comments Nucl. Part. Phys. **22**, 77 (1996).
[15] J. P. Jeukenne, A. Lejeune, and C. Mahaux, Phys. Rev. C **16**, 80 (1977).
[16] A. M. Kobos, B. A. Brown, P. E. Hodgson, G. R. Satchler, and A. Budzanowski, Nucl. Phys. **A384**, 65 (1982).
[17] A. M. Kobos, B. A. Brown, R. Lindsay, and G. R. Satchler, Nucl. Phys. **A425**, 205 (1984).
[18] M. E. Brandan and G. R. Satchler, Nucl. Phys. **A487**, 477 (1988).
[19] Dao T. Khoa and W. von Oertzen, Phys. Lett. B **304**, 8 (1993).
[20] Dao T. Khoa and W. von Oertzen, Phys. Lett. B **342**, 6 (1995).
[21] Dao T. Khoa, W. von Oertzen, H. G. Bohlen, G. Bartnitzky, H. Clement, Y. Sugiyama, B. Gebauer, A. N. Ostrowski, Th. Wilpert, M. Wilpert, and C. Langner, Phys. Rev. Lett. **74**, 34 (1995).
[22] Dao T. Khoa, W. von Oertzen, and A. A. Ogloblin, Nucl. Phys. **A602**, 98 (1996).
[23] Dao T. Khoa, W. von Oertzen, and H. G. Bohlen, Phys. Rev. C **49**, 1652 (1994).
[24] H. A. Bethe, Annu. Rev. Nucl. Sci. **21**, 93 (1971); W. D. Myers, Nucl. Phys. **A204**, 465 (1973).
[25] H. J. Gils, E. Friedman, H. Rebel, J. Buschmann, S. Zagromski, H. Klewe-Nebenius, B. Neumann, P. Pesl, and G. Bechtold, Phys. Rev. C **12**, 1239 (1980).
[26] R. C. Fuller, Phys. Rev. C **12**, 1561 (1975).
[27] H. J. Gils, Nucl. Phys. **A473**, 111 (1987); C. J. Batty, E. Friedman, H. J. Gils, and H. Rebel, Adv. Nucl. Phys. **19**, 1 (1989).
[28] G. R. Satchler, Nucl. Phys. **A409**, 3c (1983).
[29] E. D. Baron, J. Cooperstein, and S. Kahana, Phys. Rev. Lett. **55**, 126 (1985); Nucl. Phys. **A440**, 744 (1985).
[30] F. D. Swesty, J. M. Lattimer, and E. S. Myra, Astrophys. J. **425**, 195 (1994).
[31] G. F. Bertsch and S. Das Gupta, Phys. Rep. **160**, 198 (1988); W. Cassing, V. Metag, U. Mosel, and N. Nitta, *ibid.* **188**, 363 (1990); J. Aichelin, *ibid.* **202**, 233 (1991).
[32] G. D. Westfall *et al.*, Phys. Rev. Lett. **71**, 1986 (1993).
[33] Y. Schutz *et al.*, Nucl. Phys. **A599**, 97c (1996).
[34] S. Shlomo and D. H. Youngblood, Phys. Rev. C **47**, 529 (1993).
[35] J. P. Blaizot, J. F. Berger, J. Dechargé, and M. Girod, Nucl. Phys. **A591**, 435 (1995).
[36] R. Brockmann and R. Machleidt, Phys. Rev. C **42**, 1965 (1990).
[37] X. Campi and A. Bouyssy, Phys. Lett. **73B**, 263 (1978).
[38] M. El-Azab Farid and G. R. Satchler, Nucl. Phys. **A438**, 525 (1985).
[39] G. R. Satchler, Nucl. Phys. **A329**, 233 (1979).
[40] G. R. Satchler and Dao T. Khoa, Phys. Rev. C **55**, 285 (1997).
[41] M. H. Macfarlane and S. C. Pieper, Argonne National Laboratory Report No. ANL-76-11 (1978); M. Rhoades-Brown, M. H. Macfarlane, and S. C. Pieper, Phys. Rev. C **21**, 2417 (1980); **21**, 2436 (1980).
[42] G. Hauser, R. Löhken, H. Rebel, G. Schatz, G. W. Schweimer, and J. Specht, Nucl. Phys. **A128**, 81 (1969).
[43] S. Wiktor, C. Mayer-Böricke, A. Kiss, M. Rogge, P. Turek, and D. Dabrowski, Acta Phys. Pol. B **12**, 491 (1981); A. Kiss, C. Mayer-Böricke, M. Rogge, P. Turek, and S. Wiktor, J. Phys. G **13**, 1067 (1987).
[44] H. P. Gubler, U. Kiebele, H. O. Meyer, G. R. Plattner, and I. Sick, Nucl. Phys. **A351**, 29 (1981).
[45] H. Rebel, R. Löhken, G. W. Schweimer, G. Schatz, and G.

Hauser, Z. Phys. A **256**, 258 (1972).
[46] J. Albinski *et al.*, Nucl. Phys. **A445**, 477 (1985).
[47] L. W. Put and A. M. J. Paans, Nucl. Phys. **A291**, 93 (1977).
[48] V. Corcialciuc, H. Rebel, P. Pesl, and H. J. Gils, J. Phys. G **9**, 177 (1983).
[49] M. S. Hussein, A. J. Baltz, and B. V. Carlson, Phys. Rep. **113**, 133 (1984); M. S. Hussein and K. W. McVoy, Prog. Part. Nucl. Phys. **12**, 103 (1984).
[50] U. Atzrott, P. Mohr, H. Abele, C. Hillenmayer, and G. Staudt, Phys. Rev. C **53**, 1336 (1996).
[51] I. Sick, J. S. McCarthy, and R. R. Whitney, Phys. Lett. **64B**, 33 (1976).
[52] G. Bartnitzky *et al.*, Phys. Lett. B **365**, 23 (1996).
[53] K. W. McVoy and M. E. Brandan, Nucl. Phys. **A542**, 295 (1992); M. E. Brandan, M. Rodriguez-Villafuerte, and A. Ayala, Phys. Rev. C **41**, 1520 (1990).
[54] R. G. Stokstad, R. M. Wieland, G. R. Satchler, C. B. Fulmer, D. C. Hensley, S. Raman, L. D. Rickertsen, A. H. Snell, and P. H. Stelson, Phys. Rev. C **20**, 655 (1976).
[55] M. Buenerd, A. Lounis, J. Chauvin, D. Lebrun, Ph. Martin, G. Duhamel, J. C. Gondran, and P. de Saintignon, Nucl. Phys. **A424**, 313 (1984).
[56] M. E. Brandan, A. Menchaca-Rocha, M. Buenerd, J. Chauvin, P. de Saintignon, G. Duhamel, D. Lebrun, P. Martin, G. Perrin, and J. Y. Hostachy, Phys. Rev. C **34**, 1484 (1986).
[57] P. Roussel, N. Alamanos, F. Auger, J. Barrette, B. Berthier, B. Fernandez, L. Papineau, H. Doubre, and W. Mittig, Phys. Rev. Lett. **54**, 1779 (1985).
[58] A.A. Ogloblin *et al.* (unpublished).
[59] A. M. Kobos, M. E. Brandan, and G. R. Satchler, Nucl. Phys. **A487**, 457 (1988).
[60] M. E. Brandan and G. R. Satchler, Phys. Lett. B **256**, 311 (1991).
[61] Dao T. Khoa, G. R. Satchler, and W. von Oertzen, Phys. Rev. C **51**, 2069 (1995).